Wall shear rates and stagnation mass transfer on a plate in axisymmetric and cross impinging jets

Amina Meslem, Magdalena Kristiawan, I. Nastase, V. Sobolik

Wall shear rates and stagnation mass transfer on a plate in axisymmetric and cross impinging jets

A Meslem[1], **M Kristiawan**[1], **I Nastase**[2], **V Sobolik**[1]
[1] LaSIE, University of La Rochelle, Pôle Sciences et Technologie, Michel Crépeau Av., 17042, La Rochelle, France
[2] CAMBI, Technical University of Civil Engineering, 66 Pache Protopopescu Av., Bucharest, Romania

E-mail: ameslem@univ-lr.fr

Abstract. This article presents a study on the stagnation wall shear rate and mass transfer of impinging jets on a flat plate. The performance of a cross-shaped orifice nozzle was compared with a reference convergent circular nozzle having similar equivalent diameter. An array of electrodiffusion micro probes inserted into the plate was used for wall shear rates measurements. Mass transfer in the impinging region was calculated from the measured wall shear rates for a Reynolds number around 5500 and over a range of streamwise distances between the nozzle and the impinging plane within 1 to 5 nozzle equivalent diameters. The most important observation in the present investigation is that the wall shear rates and the mass transfer in the impingement region of the cross-shaped orifice nozzle are up to 175% and 40%, respectively, higher than that of the convergent nozzle. The performance of the cross-shaped orifice jet is probably related to its particular vortex dynamics characteristic of the near exit region. All the results confirm that the jet passive control enhance the mass transfer.

1. Introduction

Impinging jets are widely used in industrial processes when high heat and mass transfer rates are required. When a liquid jet strikes a surface, thin hydrodynamic, thermal and concentration boundary layers form in the region directly beneath due to the jet deceleration and the resulting increase in pressure. The thickness of the boundary layers in the stagnation region may be of the order of tens of micrometers [1]. Consequently, very high heat and mass transfer coefficients are characterizing the stagnation zone directly under the jet.

Both circular and linear impinged liquid jets studies, in single and multiple jets configurations have been widely reported in the literature. Reviews on the heat and mass transfer in impinging flows as well as variables and boundary conditions of heat and mass transfer and the influence of outlet flow conditions on transfer coefficients may be found in [2] for single jets and arrays of round or linear jets. A review of heat transfer data for single circular impinging jet was also given by in the reference [3]. Instability of the free shear layer downstream of the nozzle exit and turbulence development in the jet near field, are of fundamental importance in mass and heat transfer of impinging jet. Gardon and Akrifat [4], have studied the effect of turbulence on the heat transfer between two-dimensional jet and flat plate. It was shown that some seemingly anomalous heat-transfer phenomena can be explained as

[1] To whom any correspondence should be addressed.

effects of the turbulence occurring in jets. Turbulence is generated by the jets themselves and by possible external disturbances and varies significantly with the nozzle shape, the upstream conditions and the position within the jet. The results presented by these authors suggest that details of the nozzles, and of the upstream flow facility, may be important in the design of heat transfer equipment in which turbulent jets impinge at relatively short nozzle-to-plate spacing *H/d*, but are secondary if impingement occurs beyond $H/d = 8$.

There are several studies on the mass transfer between a plate and an impinging jet using limiting diffusion current technique. The study of Chin and Tsang [5] considered the mass transfer between an impinging jet and a circular disk electrode located in the stagnation region of the flow. They found that the electrode possesses a property of "uniform accessibility" to the diffusing species if the electrode radius is less than one nozzle diameter for the turbulent jet and half a nozzle diameter for the laminar jet. The authors have presented semi empirical correlations in both laminar and turbulent flow regimes for nozzle-to-plate distances from 0.2 to 6 nozzle diameters. The wall jet region was found to begin approximately at a radial distance of four nozzle diameters.

Yapici et al. [6] measured the surface distributions of the local shear stress values for a fully developed turbulent velocity profile, round, submerged jet, impinging on a flat surface. The results showed that the normalized local shear stresses values decreased with increasing Reynolds number and had a tendency to converge at higher Reynolds numbers. Vallis et al. [7] studied mass transfer coefficient and wall shear stress in the wall jet region for a range of Reynolds numbers between 5000 and 30000 and for nozzle to plate distance in the range 5 to 20 nozzle diameters. Alekseenko and Markovich [8] measured wall shear stresses of circular jet at a Reynolds number of 41600 and for nozzle-to-plate distances from 2 to 8 nozzle diameters. Baleras et al. [9] studied the effect of the normal velocity on the segment currents of a three-segment circular probe in the vicinity of stagnation point at Reynolds number 640. A critical survey of different methods used for the measurements of wall shear stress was made by Phares et al. [10]. He concluded that the electrodiffusion method provides the greatest accuracy of any indirect method.

No study on the wall shear stress and mass transfer for a lobed impinging jet using the electrodiffusion technique is known to the authors. Lobed jets were widely investigated for passive control of jet flows in order to improve combustion efficiency, to reduce pollutants in mixing chambers and to attenuate ejectors noise in aircraft [11,12]. Also, these jets flows were recently proposed as an efficient tool for mixing improvement in Heating, Ventilation, and Air Conditioning (HVAC) applications [13, 14]. The previous studies of lobed jets at low Reynolds numbers (< 10000) in the context of HVAC applications, allowed establishing a physical link between the induction phenomenon in the near exit region of the orifice jet and the vortical dynamics that occurs in that region. It was shown that the entrained flow rate in the near exit region of the cross-shaped lobed jet is about twice as large compared to the one of the circular reference jet. The natural instability measured at the nozzle lip of the cross-shaped orifice jet was found twice as large as of the reference round jet. Furthermore, the resulting primary Kelvin–Helmholtz (K-H) vortices are smaller in the lobed jet compared to the circular jet having the same equivalent diameter. Unlike the circular jet, where the primary rings are continuous, the K-H vortices in the lobed orifice jet flows were found to be discontinuous. The discontinuous nature of the K–H vortices enables the development of secondary streamwise structures, non-influenced by their passage as in the case of a circular jet. This way, at the troughs of each elementary cross-shaped orifice, large scale streamwise structures develop continuously and generate a complex three-dimensional distortion that results in an axis-switching, i.e. a 45°-like rotation of the initial cross-shaped transverse field. These phenomena control turbulence enhancement, air induction and flow expansion in the near field of lobed jets [14]. It is believed that the aforementioned mechanism results from self-induced Biot–Savart deformation of vortex rings due to nonuniform azimuthal curvature [15].

Since the lobed orifice jet is characterized by intensified vortical dynamics and turbulent kinetic energy in its initial region, it is believed that such a complex jet flow will also display enhanced mass transfer when considered in impinging configuration. Thus, in the present study we compare, in terms

of mass transfer rates, a cross-shaped orifice nozzle to a reference convergent circular nozzle having close equivalent diameter. The knowledge issued from previous analysis of the near field of a cross-shaped orifice jet in free air-air jet configuration [14], is used in an attempt to gain insight into the differences observed for the two studied impinging jets. Indeed, different variations of the radial distribution of wall shear rates and of the mass transfer at the stagnant point were obtained with the lobed nozzle flow relatively to the flow generated by the classical circular convergent nozzle. The wall shear rate of the impinging jets on a flat plate was measured by electrodiffusion technique and mass transfer was calculated from these values in the impingement region.

2. Experimental setup and method

2.1. Experimental setup

A schematic diagram of the apparatus used is shown in Figure 1. A gear pump (from Ismatec with a GJ-N23 head) draws its supply from the reservoir and delivers the electrolyte to the nozzle. The fluid impinges the circular target disc equipped with electrodes (Figure 1c). The temperature of the fluid is controlled by a cooling coil within ± 0.2°C. The nozzle is screwed to a 200 mm length stainless steel tube with the inner and outer diameters of 15 and 20 mm, respectively. A honeycomb manufactured of 7 mm thick disc by drilling 17 holes with a diameter of 2 mm was fitted in the tube inlet. The nozzle assembly was located in a support which allowed vertical movement for accurate alignment of the nozzle axis with the electrodes centre. The reservoir was placed on the sliding compound table (Proxxon KT 150) which permitted movement in the axial and transverse direction of the tube with a precision of 0.05 mm.

The electrodes were fabricated of a 0.5 mm platinum wire which was coated electrophoretically with a deposit of a polymeric paint. The platinum wires were used for the measurements of wall shear rate and the platinum foil with a diameter of 50 mm and thickness 50 µm as anode. The electrode positions in the target disc are shown in Figure 1c.

The test fluid was a 20 mol/m^3 equimolar potassium ferri/ferrocyanide aqueous solution with 1.5 % mass K2SO4 as supporting electrolyte. The density of the solution was 1007 kg/m3, kinematic viscosity 1.065×10^{-6} m^2/s and diffusivity 7.5×10^{-10} at 20 °C. The resulting Schmidt number was 1333. The number of electrons involved in the electrochemical reaction was equal to 1.

Two nozzles were used (see Figure d). The convergent nozzle had the exit plane diameter of 7.80 mm with an area contraction 4:1 on a length of 17 mm. The cross orifice nozzle had an equivalent diameter of 7.64 mm. The orientation of the cross shape with respect to the electrodes was either parallel (0°), i.e. its Major Plane (MP) coincided with electrodes row axis, or the cross was turned with 45°. In this case, the minor Plane (mP) of the cross orifice nozzle coincided with electrodes row axis.

2.2. Electrodiffusion method

The electrodiffusion method is based on the measurement of the limiting diffusion current on a working electrode [16]. This technique has been developed for measuring the average rates of mass transfer and their fluctuations on a wall. The transfer area consists of a small polarized electrode flush mounted in the wall. An electrochemical redox reaction whose rate is limited by mass transfer is employed.

For the total current through a circular electrode in a viscometric flow with parallel streamlines and uniform wall shear rate γ, the formula corresponding to the Leveque's equivalent equation for heat transfer was established by [17].

$$I_L = \frac{0.884\pi}{3^{1/3}\,\Gamma(4/3)}\, n\, Fc\, \gamma^{1/3}\, D^{2/3}\, R^{5/3} \qquad (1)$$

For the mean current density it holds:

$$i_L = \frac{0.884}{3^{1/3}\,\Gamma(4/3)}\, n\, Fc\, \gamma^{1/3}\, D^{2/3}\, R^{-1/3} \tag{2}$$

In the case of an impinging circular jet, the streamlines in the wall vicinity spread radially from the stagnation point *S*. The current density in the point *P* on the electrode is expressed by the relation [9]:

$$i_D(r_P) = i^* \left[1 - \left(\frac{r_0}{r_P} \right)^3 \right]^{-1/3} \tag{3}$$

where i^* is the current density on an electrode located in stagnation point *S*. It should be emphasized that the position of the stagnation point within the electrode is arbitrary. The electrode is then uniformly accessible to the diffusion mass transfer and the thickness of the concentration boundary layer is also uniform. It holds for i^*:

$$i^* = \frac{1}{3^{1/3}\Gamma(4/3)} nFcA^{1/3}D^{2/3} \tag{4}$$

We are interested in the mass transfer on an electrode located in the impingement region and containing the stagnation point. For this aim, we shall measure the distribution of wall shear rate and calculate the parameter $A = \gamma(r)/r$, which is constant in the impingement region.
Coefficient of mass transfer is expressed as:

$$k = \frac{i^*}{nFC} = \frac{A^{1/3}D^{2/3}}{3^{1/3}\Gamma(4/3)} \tag{5}$$

Sherwood number is defined as:

$$Sh = \frac{k\,d}{D} = \frac{1}{3^{1/3}\Gamma(4/3)} \left(\frac{A}{D} \right)^{1/3} d \tag{6}$$

where *d* is the diameter of the nozzle. The hydrodynamic parameter *A*, the coefficient of diffusion *D*, and the diameter of nozzle *d*, are sufficient for the calculation of the Sherwood number in the impingement region.
For the evaluation of *A*, it is necessary to calculate γ from the measured limiting current. The Leveque equation (Eq. 1) was derived under the assumption of parallel streamlines and uniform wall shear rate. The streamlines in the impingement region are radial and the wall shear rate increases with *r*. More details on the measuring method can be found in the reference [18].

3. Results and discussion

The nozzle axis was adjusted into the point A_p of the target disc (see Figure 1c). Then the nozzle was moved away from the target point at an assigned nozzle-to-plate axial distance *H*. Sixteen measurements were carried out at one axial distance *H*, by horizontal displacement of the stagnation point from the point A_p to the point B_p, in fifteen steps of 1 mm. The currents of 6 electrodes were sampled at a frequency of 100 Hz during 10 s for every measurement. In this way, we obtained several values of the current measured by different electrodes at similar radial distances from the stagnation point. Wall shear rates γ were calculated from the measured currents using Eq. 1.

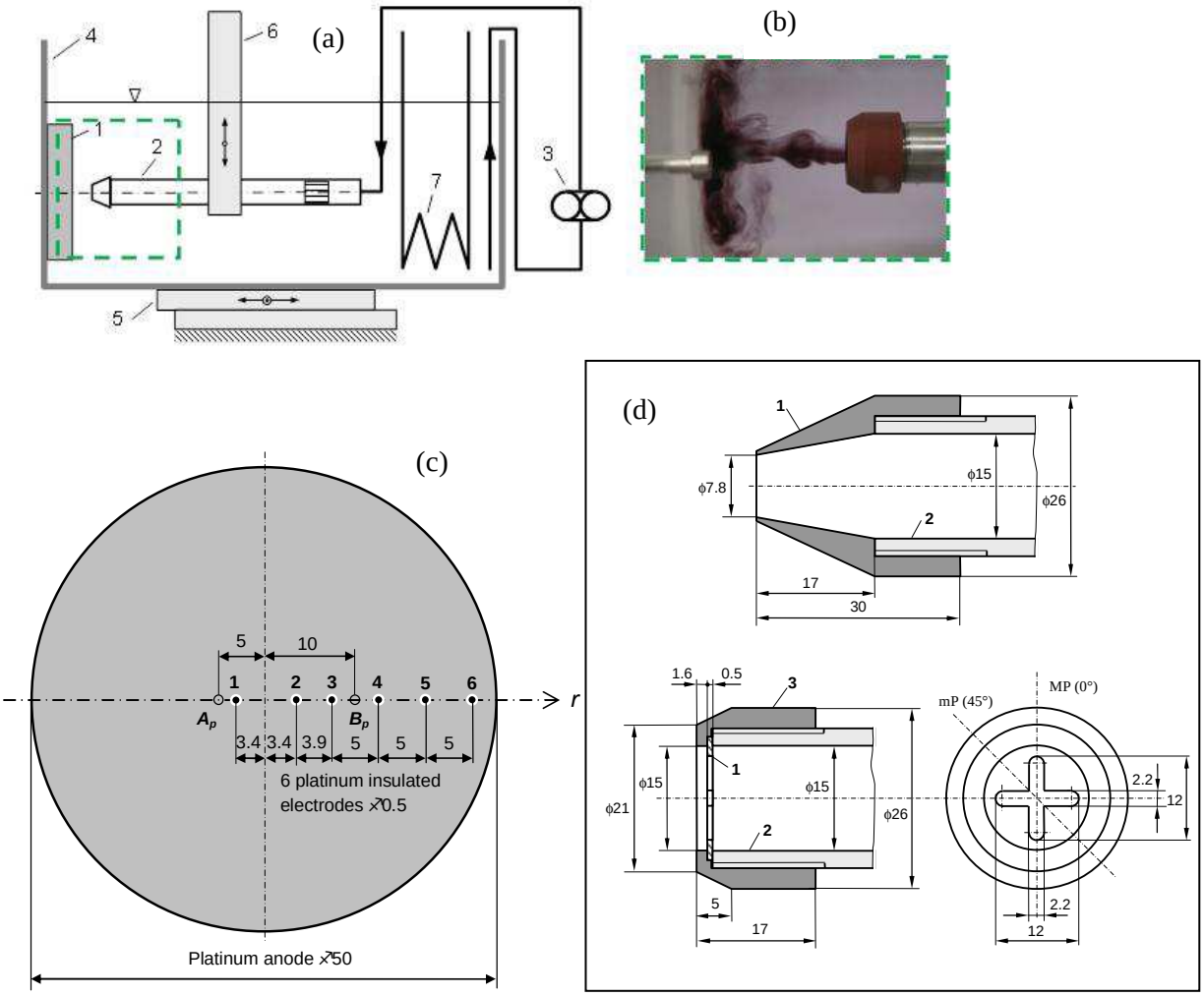

Figure 1: (a) Experiment setup: 1 target disc with electrodes, 2 tube with nozzle and honeycomb, 3 pump, 4 reservoir, 5 compound table, 6 nozzle holder, 7 cooling coil. (b) Visualization of impinging jet. (c) Target disc with electrodes row: 1-6 electrodes ϕ 0.5mm; A_p, B_p limits of stagnation point displacement. (d) Nozzles geometries (top: 1 - convergent circular nozzle, 2 – tube; down: 1 – cross orifice, 2 – tube, 3 – sleeve nut)

An example of γradial distribution is given for $H = 1d_e$ in Figure 2a. In the cross-shaped jet, very high maximum is achieved (22000 s^{-1}) when the MP of the orifice was aligned with the electrodes (position 0°). At this position the maximum wall shear rate induced by the cross orifice nozzle is up to 175% higher than the maximum of the circular nozzle. Examining Figure 2a, it can be seen that the variation pattern of the local wall shear rates of impinging cross-shaped jet has a particular shape in the MP. The maximum is at r of about 6 mm (0.8 d_e) which corresponds to the aperture extremity. Outside of this maximum, γ diminish rapidly and its values are lower in both stagnation and wall jet regions than for the other distances H (not shown). It can be observed that the curve is not straight in the vicinity of the stagnation point at this position. There are two slopes separated by an inflection point around $r = 0.4\ d_e$ which could be explained by the inflection point in the streamwise velocity profile U, in the MP of the jet near field at the same radial position $r = 0.4\ d_e$ (Figure 2b). Inflection point in U-profile in the MP is related to the inner shear layer at the junction of the central jet core and its lobes. It is expected that velocity gradient in the MP generated flow acceleration in lobe regions as the jet approached the target plate and consequently induced very high wall shear rates in these regions.

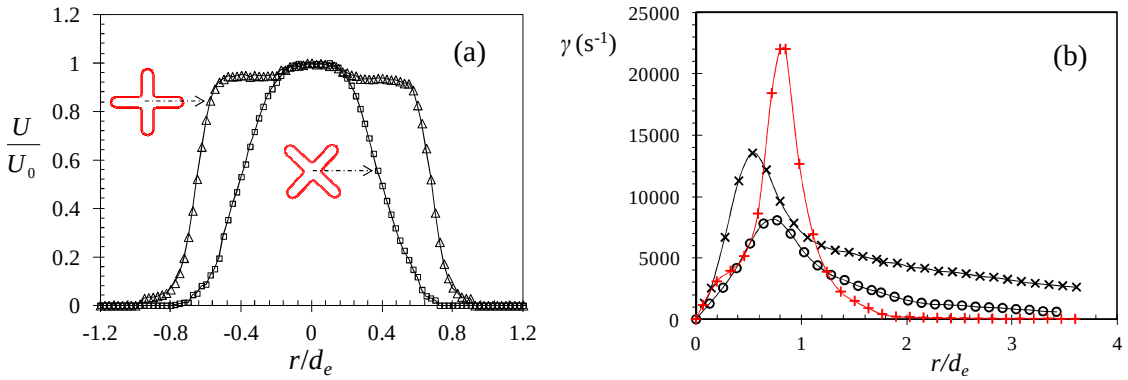

Figure 2: (a) Streamwise velocity profiles in the near field of the cross shaped orifice air-air nozzle jet [14]. (b) Wall shear rate for H=1d_e. Symbols: ○ for circular convergent nozzle, + for cross-shaped orifice nozzle-MP and × for cross-shaped orifice nozzle-mP.

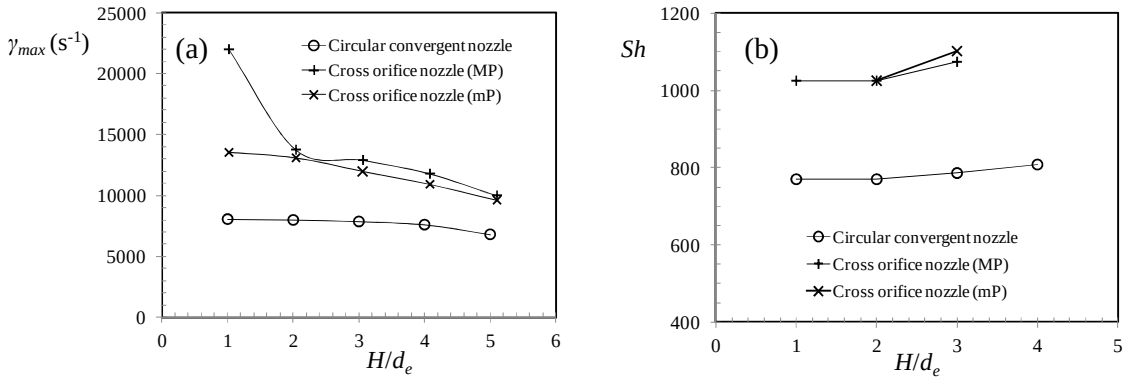

Figure 3: (a) Maximum wall shear rate as a function of H/de Sherwood number in the stagnation region as a function of H/d_e. (b) Sherwood number in the stagnation region as a function of H/d_e.

When the orifice is lobed-shaped as in the present study, it is expected that the wall shear rate and mass transfer in the jet near field are less dominated by K-H structures since they are smaller and discontinuous [14]. The lobed geometry promotes the breakdown of K-H structures and increases the jet mixing by streamwise structures enhancement. Streamwise structures which increase the turbulent kinetic energy in the jet near field have probably a dominant role in wall shear rates and mass transfer improvement.

The values of γ for the cross orifice nozzle remain superior to the circular nozzle for all the explored positions H (Figure 3a). This significant difference allows us to confirm the hypothesis of a considerable interest for the passive control of impinging jets for mass transfer enhancement. The changes in the nozzle geometry modify the wall shear rates and mass transfer to the impinging jet because they affect the development of the jet before it impinges on the plate.

When the radial profile of $\gamma$is straight in the vicinity of the stagnation point (i.e. for H≥1d_e, the curves are not shown for brevity), the wall shear rates were fitted with linear dependence in the stagnation region. The slope of these straight lines is equal to the hydrodynamic parameter A according to the equation $\gamma = \partial u / \partial z\big|_{z=0} = Ar$. The slopes found for the cross nozzle jet are superior to the slopes in the case of the circular jet, but the observed radius of the impingement region of the cross nozzle jet was smaller than of the circular jet. This is consistent with the characteristic *vena contracta* phenomenon in the near field of the right-angle orifice jets. The results on Sherwood number (Eq. 6) calculated from A for different nozzles using the equivalent diameter d_e are shown in Figure 3b. The

mass transfer in the impingement region of the cross nozzle jet is up to 40% higher than in the circular jet issuing from the convergent nozzle.

The frequency content of the polarographic signals is obtained from studying the energy spectra for different nozzle-to-plate distances (Figure 4). In the lobed jet (Figure 4a) the spectrum is noisy and the frequency peaks f_n, which are related to the Kelvin–Helmholtz (K-H) dynamics, are function of H/d_e (Figure 4c) due to Biot–Savart phenomenon deformation of vortex rings [19]. Due to the small size of the K-H structures in the lobed jet, their contribution in mass transfer is expected to be negligible. The mass transfer in the lobed jet is probably dominated by large streamwise structures which develop in orifice troughs [14]. Conversely, in the circular jet, the periodic K-H rings with a frequency of f_n =52.4 Hz for $H \leq 4\ d$ (Figure 4b and c) are the main features, which affect the mass transfer.

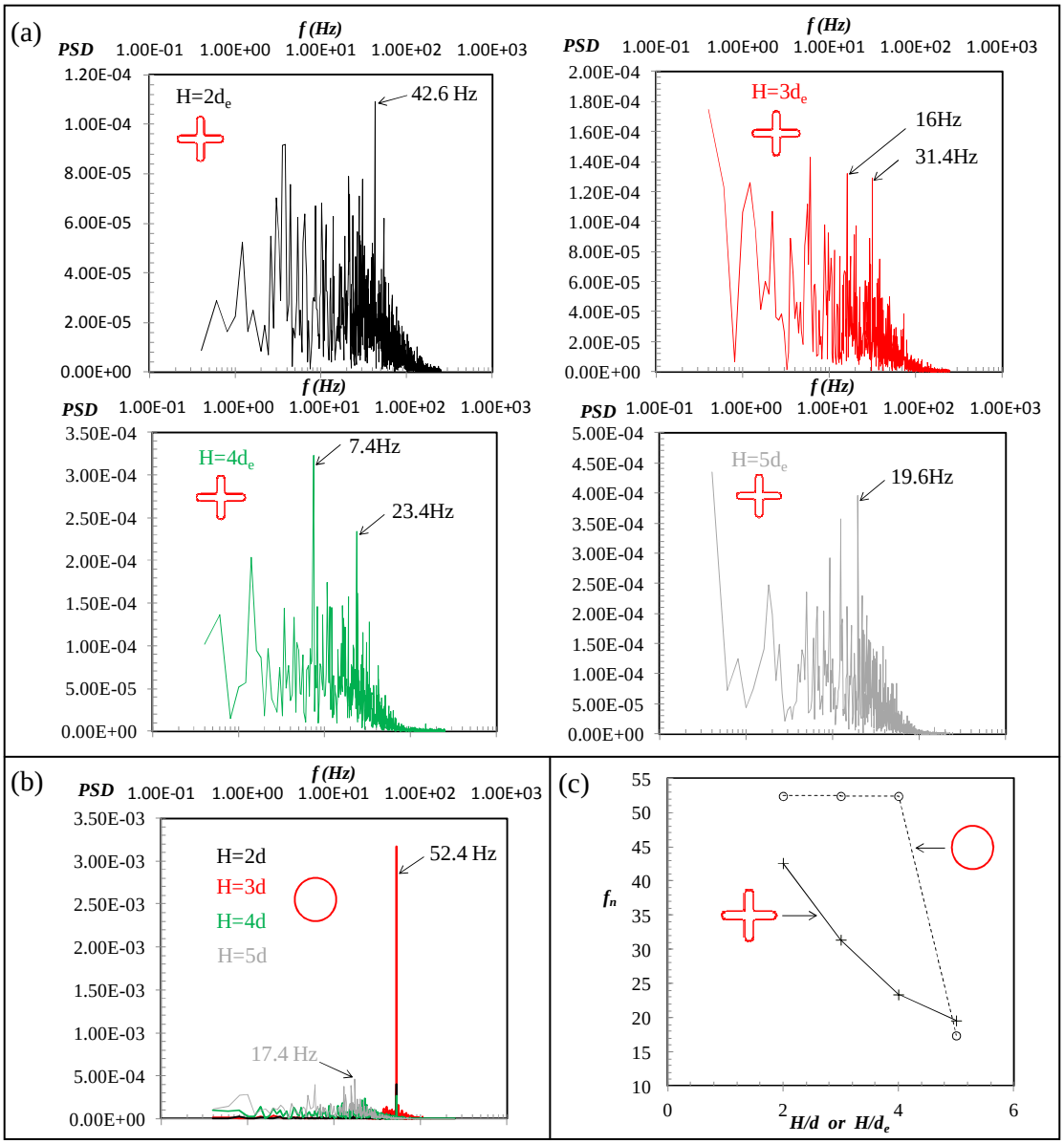

Figure 4: (a, b) Energy spectra of the wall shear stress fluctuations for cross orifice nozzle and for convergent nozzle respectively. (c) K-H vortex frequency as a function of nozzle-to plate distance.

At the end of the potential core region of the circular jet ($H = 5\ d$), the frequency is one third of the K-H vortex frequency. This is probably due to the fusion of three K-H rings during pairing phenomenon.

4. Conclusions

In this study a cross-shaped orifice nozzle impinging jet was compared to a reference circular nozzle jet in terms of wall shear rate and mass transfer capabilities. The mass transfer in the stagnation zone of the cross nozzle for H/d_e in the interval (2, 3) is independent of the cross angle and is up to 40% higher than the mass transfer of the circular nozzle.

The wall shear rate achieved a high level maximum along the Major Plane for nozzle-to-plate distance $H = 1\ d_e$. At this distance the maximum wall shear is up to 175% higher than of the circular nozzle. Downstream this position, the wall shear rate becomes independent of the rotation angle of the cross and the maximum values remain superior to the circular nozzle. At $H = 2\ d_e$ the wall shear rate with the cross orifice nozzle is 75% higher than the one of the circular nozzle.

The changes in the nozzle geometry modify the wall shear rates and mass transfer to the impinging jet due to the fact that they are affecting the development of the jet before it impinges on the plate.

The knowledge issued from the previous analysis of the region in the near field of a cross-shaped orifice jet in free air-air jet configuration, was used in the present study. This explains the differences observed for the radial distributions of wall shear rates and mass transfer at the stagnant point in the two cases.

In the case of the circular jet, wall shear rate and mass transfer are dominated by the large-scale K-H structures which appear downstream the nozzle exit plane. This is not the case for the cross shaped orifice jet for which the K-H structures are smaller and discontinuous. The lobed geometry promotes the breakdown of K-H structures and increases the jet mixing through the particular dynamics of the generated streamwise structures. These particular vortices which increase the turbulent kinetic energy in the jet near field probably play a dominant role in wall shear rates and mass transfer improvement.

The obtained results allow us to confirm the hypothesis of a considerable interest for the passive control of impinging jets as a method of mass transfer enhancement.

References

[1] Webb, B.W. and Ma, C.F. 1995 *Advances in Heat Transfer* **26** 105
[2] Martin, H. 1977 *Advances in Heat Transfer* **13** 1
[3] Jambunathan, K. et al. 1992 *Int. J. Heat and Fluid Flow* **13** 106
[4] Gardon, R. and Akfirat, J.C. 1965 *Int. J. Heat and Mass Transfer* **8** 1261
[5] Chin, D.T. and Tsang, C.H. 1978 *J. Electrochemical Society* **125** 1461
[6] Yapici, S., et al. 1999 *J. Appl. Electrochemistry* **29** 185
[7] Vallis, E.A., Patrick, M.A. and Wragg, A.A 1977. Techniques of wall measurements in fluid mechanics. *in Euromech 90* Nancy, France.
[8] Alekseenko, S.V. and Markovich, D.M. 1994 *J. Appl. Electrochemistry* **24** 626
[9] Baleras, F., et al. 1994 *J Appl. Electrochemistry* **24** 676
[10] Phares, D.J., Smedley G.T., and Flagan, R.C 2000. *J. Fluid Mechanics* **418** 351
[11] Karagozian, A.R., *Lecture Notes in Control and Information Sciences. Control of Fluid Flow* 2006 **330** 75
[12] Mi, J., Kalt, P. and Nathan, G. J. 2010 *Flow Turbulence Combust* **84** 565
[13] Meslem, A., Nastase, I., and Allard, F. 2010 *Build. Environment* **45** 2679
[14] Nastase, I., Meslem, A. and Gervais, P. 2008 *Exp. Fluids*. **44** 1027
[15] Gutmark, E.J., et al. 1989 *Exp. Fluids* (Suppl.) **7** 248
[16] Selman, J.R. and Tobias, C.W. 1978 *Advances Chem. Eng. J.* **10** 211
[17] Reiss, L.P. and Hanratty, T.J. 1962 *Advances Chem. Eng. J.* **8** 245
[18] El Hassan et al. 2012 *Exp. Fluids* **52** 1475
[19] Gutmark, E. J. et al. 1989 *Exp. Fluids*. **7** 248